3D Control of Rotating Millimeter-Scale Swimmers Through Obstacles

Julien Leclerc, Haoran Zhao, and Aaron T. Becker

Abstract—This study investigates the high speed 3D navigation of rotating millimeter-scale swimmers. The swimmers have a spiral-shaped surface to ensure propulsion. The rotational movement is used for propulsion and, in future work, could provide the power needed to remove blood clots. For instance, an abrasive tip could be used to progressively grind a blood clot.

An algorithm to perform 3D control of rotating millimeterscale swimmers was implemented and tested experimentally. The swimmers can follow a trajectory and can navigate without touching the walls inside a tube having a diameter of 15 mm. This diameter is smaller than the average diameter of the distal descending aorta, which is the smallest section of the aorta. Several swimmers designs were built and tested. The maximum velocity recorded for our best swimmer was 103.6 mm/s with a rotational speed of 477.5 rotations per second.

I. INTRODUCTION

Magnetically actuated millimeter-scale swimmers could be used in surgery to reduce the invasiveness of certain procedures. Because the human body is effectively transparent to low frequency magnetic fields, a magnetic swimmer inserted inside a person can be controlled by an external magnetic field without the need for wires or tethers. Such magnetic swimmers contain a piece of magnetic material (permanent magnet or ferromagnetic material). The external magnetic field can, therefore, apply a force and/or a torque to the swimmer from a distance. A magnetic manipulator can be used to generate a controlled external magnetic field.

Arterial embolism and arterial thrombosis are two conditions in which an occlusion prevents blood from flowing adequately inside an artery. These conditions may result in an *ischemia* (shortage of the oxygen supplied to an organ) and lead to an *infarction* (tissue damage due to an insufficient blood supply). A *thrombosis* is a clot formed by blood coagulation. An *embolism* is caused when an object traveling inside the bloodstream reaches a vessel that is too narrow for it to pass through. Most organs can be affected by an ischemia: the heart (myocardial or cardiac ischemia), the brain (cerebral ischemia), the leg (limb ischemia), the small intestine (mesenteric ischemia), etc.

Arterial occlusions can be removed using a catheter [1]. These devices are tubes inserted inside an artery and guided toward the occlusion to remove. Different tools can be inserted into the catheter to perform the occlusion removal.

Miniature magnetic swimmers could be used to remove arterial clots as in [2]–[5]. In [2] the authors used a helical

The authors thank https://mynsmstore.uh.edu/ for printing the swimmers used in this study. Authors are with the Dept. of Electrical and Computer Engineering, University of Houston, Houston, TX 70004, USA, jleclerc@uh.edu Work was partially supported by National Science Foundation IIS-1553063, IIS-1619278 and CNS-1646566.

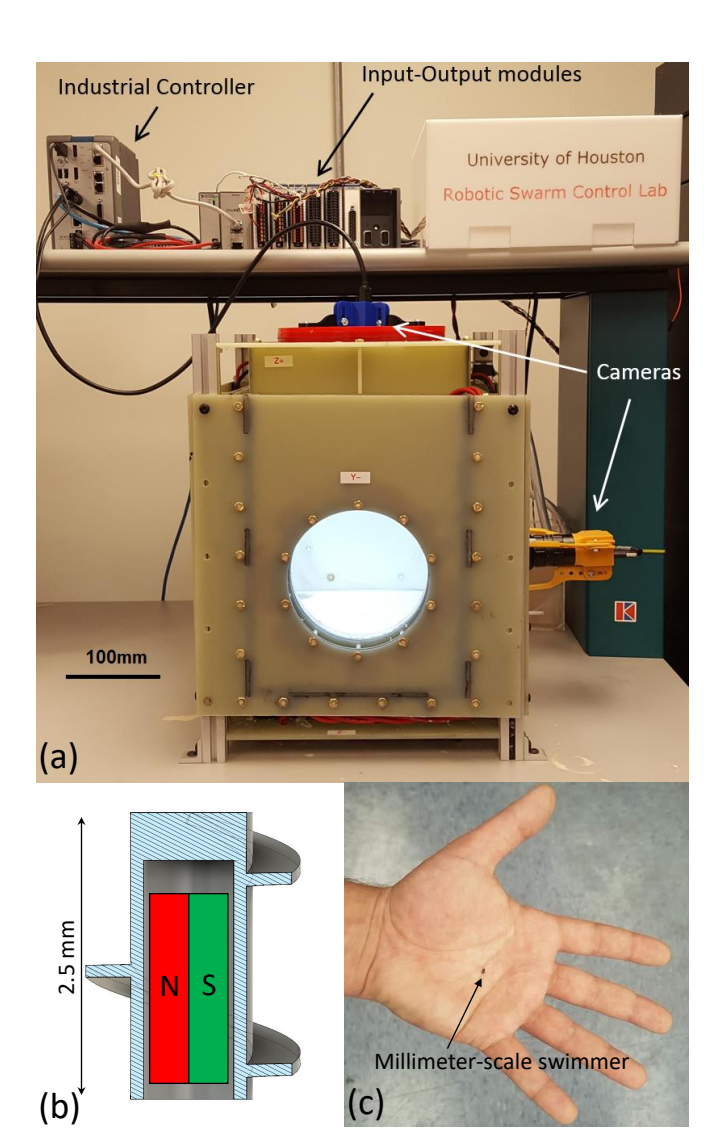


Fig. 1. (a) Picture of the magnetic manipulator used to control the millimeter-scale swimmer. (b) CAD drawing of a magnetic swimmer. (c) Picture of a miniature swimmer held by the first author.

microswimmer to rub against blood clots. The microswimmer contained a permanent magnet and an external rotating magnetic field was applied to make it rotate. It had a length of 2.2 mm and a diameter of 0.346 mm. The rotation of the microswimmer is used for both propulsion and clot removal. The end of its helical tail was rubbed against the clot and was able to achieve a clot removal rate of 0.56 mm³/s with a rotational speed of 35 Hz. It could reach a velocity of 26 mm/s when free swimming.

Rotating microswimmers have also been proposed to perform micro manipulation [6], or deliver medication [7]–[10].

Several groups have built and tested miniature swimmers having sizes ranging from the micrometer to the centimeterscale. In [11] and [7] the authors built and tested 16 µm long helical swimmers designed to perform localized medication delivery. A helical swimmer having a length of 7 µm is presented in [12]. This swimmer reached a velocity of 40 µm/s at a rotational speed of 150 Hz. In [13] the authors study the swimming characteristics of 280 µm-long helical swimmers inside fibrous environments. The fastest velocity they obtained was equal to 2.1 mm/s. Millimeter-scale rotating swimmers for medical applications were also studied [14], [15]. This prototype had a length of 15 mm and reached a velocity of 10 mm/s at a rotational speed of 28 Hz. In [9], a larger swimmer (60 µm long) was able to reach speeds up to 250 µm/s at 70 Hz. Centimeter-scale rotating swimmers were studied for navigation inside the digestive tract ([16], [17]. The helical capsule in [17] reached a velocity of 25 mm/s.

Two methods are available to produce the time-varying magnetic field needed to actuate the swimmers. Permanent magnets can be moved near the workspace using a robotic arm [18] or simply rotated around one axis. Using permanent magnets is energy efficient as no energy is consumed to generate the magnetic field. However, inertia limits system dynamics. Permanent magnets can be heavy and could cause safety issues when quickly moved next to a patient. Another option is to use electromagnets instead of permanent magnets [19]. Power is lost via Joules effect inside an electromagnet however, no moving parts are required. The magnetic field variation rate is only limited by the maximum voltage of the power supply because the magnetic flux variation is proportional to the electromotive force.

A precise, accurate and robust control method of the magnetic swimmer will be paramount to achieve safe surgery. The open-loop control of a helical swimmer with gravity compensation is presented and demonstrated in [20]. Five DOF closed-loop control of a non-rotating swimmer for eye surgery was achieved in [21] using eight electromagnets. Closed-loop control of the orientation of a helical swimmer was presented in [22]. A camera was used to measure the orientation of the swimmer and 3 Helmholtz coil pairs generated the magnetic field. In [23] the authors presented and tested a method to perform closed-loop path following using a helical swimmer.

This paper studies the navigation control of millimeterscale rotating swimmers at the size scale of large human arteries. Major arteries have a relatively large diameter (see table I) which allows navigating swimmers with diameters up to 3 mm. Increasing the diameter of the swimmer allows producing more thrust which is necessary to counteract the blood flow since blood flows at higher velocities in large arteries. In addition, the increased size allows embedding a larger volume of permanent magnet. Because torque is proportional to magnet volume, this allows producing more torque without increasing the magnitude of the magnetic field.

This paper presents two novelties. (1) An algorithm able to

TABLE I

Non-exhaustive list of large arteries of the human body. The swimmers tested have a diameter of 2.5 mm and could navigate inside all the arteries of the table. Data were obtained from [25].

Artery name	Diameter range
Celiac trunk	6 to 8 mm
Common hepatic artery	5 to 7 mm
Gastroduodenal artery	4 to 6 mm
Inferior mesenteric artery	3 to 5 mm
Internal iliac artery	4 to 6 mm
Renal artery	5 to 7 mm
Splenic artery	5 to 8 mm
Superior mesenteric artery	6 to 8 mm

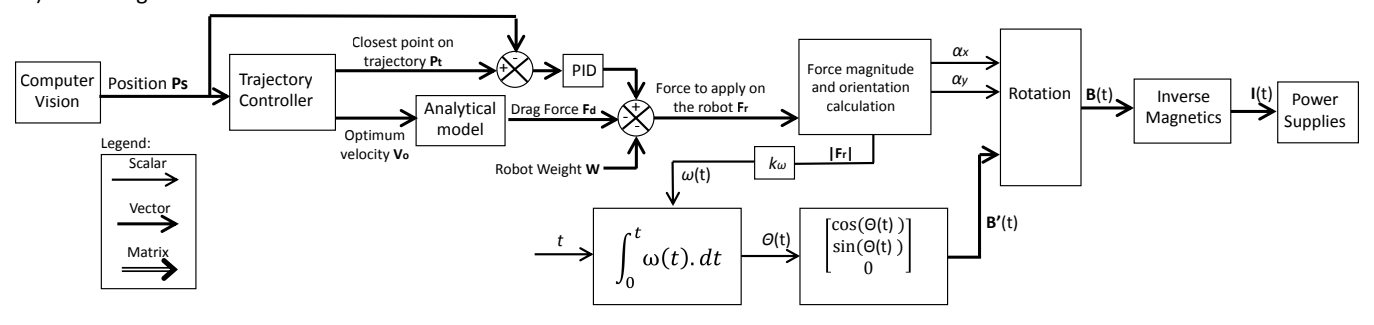
control rotating magnetic swimmers in 3D was designed and experimentally tested. The swimmers were tested in water for all experiments presented in this paper. They are able to follow a trajectory and navigate inside a tube having a diameter of 15 mm. This diameter is smaller than the average diameter of the distal descending aorta which is the smallest section of the aorta. The swimmer does not touch the walls of the tube and would, therefore, avoid any risk of detaching plaques when navigating inside the aorta. (2) Different swimmer designs were tested experimentally. They all have a diameter equal to 2.5 mm. They rotated at speeds up to 477.5 Hz and the highest velocity measured was 103.6 mm/s when going upward (against gravity). To our knowledge, such high velocities have not been achieved before with a magnetic rotating swimmer. A video presenting the device and experimentations is available for download in the media section or can be streamed at [24].

II. DESCRIPTION OF THE MAGNETIC MANIPULATOR

The magnetic manipulator uses six electromagnets to produce the magnetic field. The electromagnets are placed in a cubical shape having a side length of 300 mm. The usable workspace (volume in which a magnetic swimmer can be controlled) is a cube having a side length of 150 mm. This desktop manipulator is suitable for phantom studies on organs and limbs with diameters less than 150 mm. The design is parametric and a study examining scaling the manipulator in size was presented in [26]. This manipulator does not produce a uniform magnetic field. Instead, an inverse magnetic calculation taking into account the nonlinearity is performed to calculate the currents to apply to the electromagnets (see subsection III-C). The electromagnets of this manipulator can be cooled using liquid nitrogen to produce higher magnetic fields. However, this feature was not used in this study.

The electromagnets are driven by high-accuracy KEPCO BOP 20-50 power supplies used in current mode. In this mode, the power supplies generate a current proportional to an analog input. A total of 12 power supplies are used. They are connected 2 by 2 in series and each pair powers an electromagnet. Each set can generate 20 A of current and

a) Block diagram of the controller



b) Block diagram of the hardware

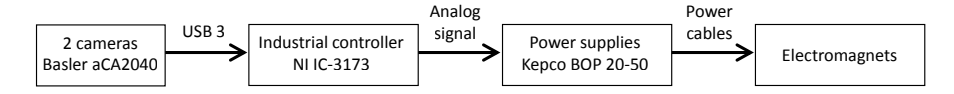


Fig. 2. a) Block diagram of the controller designed to control rotating swimmers. b) Block diagram of the hardware implementation.

apply a voltage of 100 V. The total power available is equal to 12 kW.

The analog input is computed and generated by a real-time computer IC 3173 manufactured by National Instruments [27]. Two Basler aCA2040 cameras [28] are placed on orthogonal sides of the workspace to measure the position of the swimmer in 3D at a frequency of 100 Hz. More details about this system can be found in [26]. A picture of the manipulator is presented in fig. 1.

III. CONTROLLER

The control is divided into three steps: orientation and rotational speed, magnetic field calculation, and electromagnets current calculation.

A. Swimmer orientation and rotational speed

The trajectory to follow is defined by a matrix containing the coordinates of waypoints on the trajectory centerline and the corresponding velocity setpoints. The user only has to enter a few points and the program performs an interpolation to produce a smooth trajectory profile. The trajectory in this paper uses 35 waypoints.

The position and velocity control is performed by properly orienting the vector force produced by the swimmer propulsion. The magnitude of the force is controlled by varying the rotational speed of the swimmer. The orientation of the force is determined by the orientation of the swimmer. The algorithm first must compute the force to be applied to the swimmer. The force to apply contains three components: one to compensate gravity, one to compensate the expected drag (the drag along the trajectory centerline) and one to keep the swimmer on the trajectory centerline.

The algorithm first measures the position of the swimmer. Our experimental setup uses two cameras to perform this measurement (see sec. II). The nearest point on the interpolated trajectory, **P**, is found via a search. The difference between **P** and the swimmer position is used as the input of the PID regulator shown in fig. 2. The output of the

regulator corresponds to the force component needed to keep the swimmer on the trajectory centerline.

The optimum velocity vector V at point P must then be calculated. Its direction is tangent to the trajectory centerline and its magnitude is defined in the matrix T. A simple fluid mechanics model, presented in equation 1, is used to compute the drag force F_d corresponding to this velocity vector. In this equation, C_d is the drag coefficient, ρ is the density of the fluid, V is the velocity vector and S is the cross-section area.

$$\mathbf{F_d} = -C_d \cdot \rho \cdot \mathbf{V} \cdot S \tag{1}$$

The force $\mathbf{F_r}$ produced by a rotating swimmer is always collinear to its rotational axis. The orientation of the swimmer is therefore set collinear to $\mathbf{F_r}$. The rotational speed ω is calculated from the magnitude of the force using eq. 2 where k_t is the thrust coefficient.

$$\omega = \frac{|\mathbf{Fr}|}{k_{+}} \tag{2}$$

B. Magnetic field

$$\mathbf{B}_{uvw} = \begin{bmatrix} B_u \\ B_v \\ B_w \end{bmatrix} = B_0 \cdot \begin{bmatrix} \cos(\theta(t)) \\ \sin(\theta(t)) \\ 0 \end{bmatrix}$$
(3)

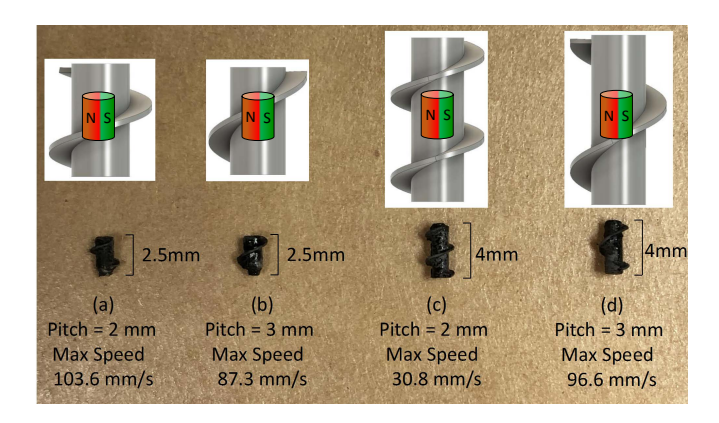


Fig. 3. Presentation of different swimmer designs tested experimentally.

$$\mathbf{R}(\alpha_x, \alpha_y) = \mathbf{R}_{\mathbf{x}}(\alpha_x) \cdot \mathbf{R}_{\mathbf{y}}(\alpha_y)$$

$$= \begin{bmatrix} 1 & 0 & 0 \\ 0 & \cos(\alpha_x) & -\sin(\alpha_x) \\ 0 & \sin(\alpha_x) & \cos(\alpha_x) \end{bmatrix} \cdot \begin{bmatrix} \cos(\alpha_y) & 0 & \sin(\alpha_y) \\ 0 & 1 & 0 \\ -\sin(\alpha_y) & 0 & \cos(\alpha_y) \end{bmatrix}$$
(4

$$\mathbf{B}_{xyz} = \mathbf{R}(\alpha_x, \alpha_y) \cdot \mathbf{B}_{uvw} \tag{5}$$

C. Electromagnets current

This subsection briefly explains how the currents to apply to each electromagnet are calculated. More detail about this method is presented in [26].

The total flux density is the sum of the flux density produced by each electromagnet. At the swimmer location, this sum must be equal to the flux density \mathbf{B}_{xyz} calculated in subsection III-B.

First, a vector **I** containing the current of each electromagnet is defined:

$$\mathbf{I} = \begin{bmatrix} I_1 & I_2 & I_3 & I_4 & I_5 & I_6 \end{bmatrix}^\top \tag{6}$$

The flux density can be calculated from the electromagnet currents using the following equation:

$$\mathbf{B}_{xuz} = \mathbf{A} \cdot \mathbf{I} \tag{7}$$

The actuation matrix **A** is defined as follows:

$$\widetilde{\mathbf{B}}_{x(\mathbf{P})} = \left[\widetilde{B}_{1x(\mathbf{P})} \ \widetilde{B}_{2x(\mathbf{P})} \ \widetilde{B}_{3x(\mathbf{P})} \ \widetilde{B}_{4x(\mathbf{P})} \ \widetilde{B}_{5x(\mathbf{P})} \ \widetilde{B}_{6x(\mathbf{P})} \right] \quad (8)$$

$$\widetilde{\mathbf{B}}_{y(\mathbf{P})} = \left[\widetilde{B}_{1y(\mathbf{P})} \ \widetilde{B}_{2y(\mathbf{P})} \ \widetilde{B}_{3y(\mathbf{P})} \ \widetilde{B}_{4y(\mathbf{P})} \ \widetilde{B}_{5y(\mathbf{P})} \ \widetilde{B}_{6y(\mathbf{P})} \right] \quad (9)$$

$$\widetilde{\mathbf{B}}_{z(\mathbf{P})} = \left[\widetilde{B}_{1z(\mathbf{P})} \ \widetilde{B}_{2z(\mathbf{P})} \ \widetilde{B}_{3z(\mathbf{P})} \ \widetilde{B}_{4z(\mathbf{P})} \ \widetilde{B}_{5z(\mathbf{P})} \ \widetilde{B}_{6z(\mathbf{P})} \right] \quad (10)$$

$$\mathbf{A} = \begin{bmatrix} \widetilde{\mathbf{B}}_{x(\mathbf{P})} \\ \widetilde{\mathbf{B}}_{y(\mathbf{P})} \\ \widetilde{\mathbf{B}}_{z(\mathbf{P})} \end{bmatrix}$$
(11)

The coefficients $B_{it(\mathbf{P})}$ represent the magnitude of the flux density produced per unit of current by EM i on axis t where t can be equal to x, y, or z. These coefficients only depend on the geometry of the manipulator and the position of the swimmer. Their coefficients are calculated using the Biot-Savart law. Details of this calculation are presented in [26].

 $\bf A$ is a 3×6 matrix. It describes an under-determined system and eq. 7 has therefore an infinite number of solutions. A pseudo-inverse is therefore calculated. It was chosen to use the least norm solution (see eq. 12) as it minimizes the norm of $\bf I$ and therefore tends to reduce power consumption.

$$\mathbf{I} = \left(\mathbf{A}^{\top} \cdot \mathbf{A}\right)^{-1} \cdot \mathbf{A}^{\top} \cdot \mathbf{B}_{xyz} \tag{12}$$

IV. MILLISWIMMER DESIGN AND FABRICATION

The milliswimmers have a spiral shape (see fig. 3). They are similar to the designs presented in [29], [30]. All swimmers tested have a diameter of 2.5 mm. They were 3D printed using a Projet 3510 HD manufactured by 3D Systems [31] and the material used was the VisiJet M3-X developed by the same company. Four different designs were built and tested (see fig. 3).

The swimmer is designed with a cup-shaped void to receive a cylindrical permanent magnet, which is glued in place with epoxy. The magnets were the same for all tested swimmers. They are made of N50 NdFeB, have a diameter of 0.75 mm and a length of 1 mm. They are radially magnetized to allow producing a torque along the revolution axis of the swimmer. The swimmers were painted black to facilitate detection by the machine vision system.

V. EXPERIMENTAL TRAJECTORY FOLLOWING

The algorithm described in section III was tested experimentally. The hand-designed goal trajectory was specified by 35 waypoints, and then automatically interpolated to 100 waypoints. This trajectory moves straight up inside a tube simulating an aorta. It exits the tube from the top and goes to the right side of the workspace. The trajectory then makes several turns to slowly bring the swimmer to the bottom of the workspace. It then re-enters the tube from the bottom. The trajectory forms a loop that the swimmer follows until halted. A 3D representation of the trajectory centerline is provided in fig. 5. This figure also presents the trajectory obtained experimentally. Additional pictures of the swimmer at different times are also provided in fig 6. The swimmer used has a pitch of 2 mm and a length of 2.5 mm. It corresponds to picture a) in fig 3. It is the best swimmer tested as explained in the following section VI.

The control law is not optimized. In particular, there is a significant error between the path centerline and the position of the swimmer when the trajectory is tortuous. However, the control is *precise* as it is approximately the same for each loop performed. The orange curve on fig. 5 corresponds to the path followed by the swimmer while accomplishing the trajectory three times in a row. The paths are almost superimposed. Future work should focus on improving path tracking.

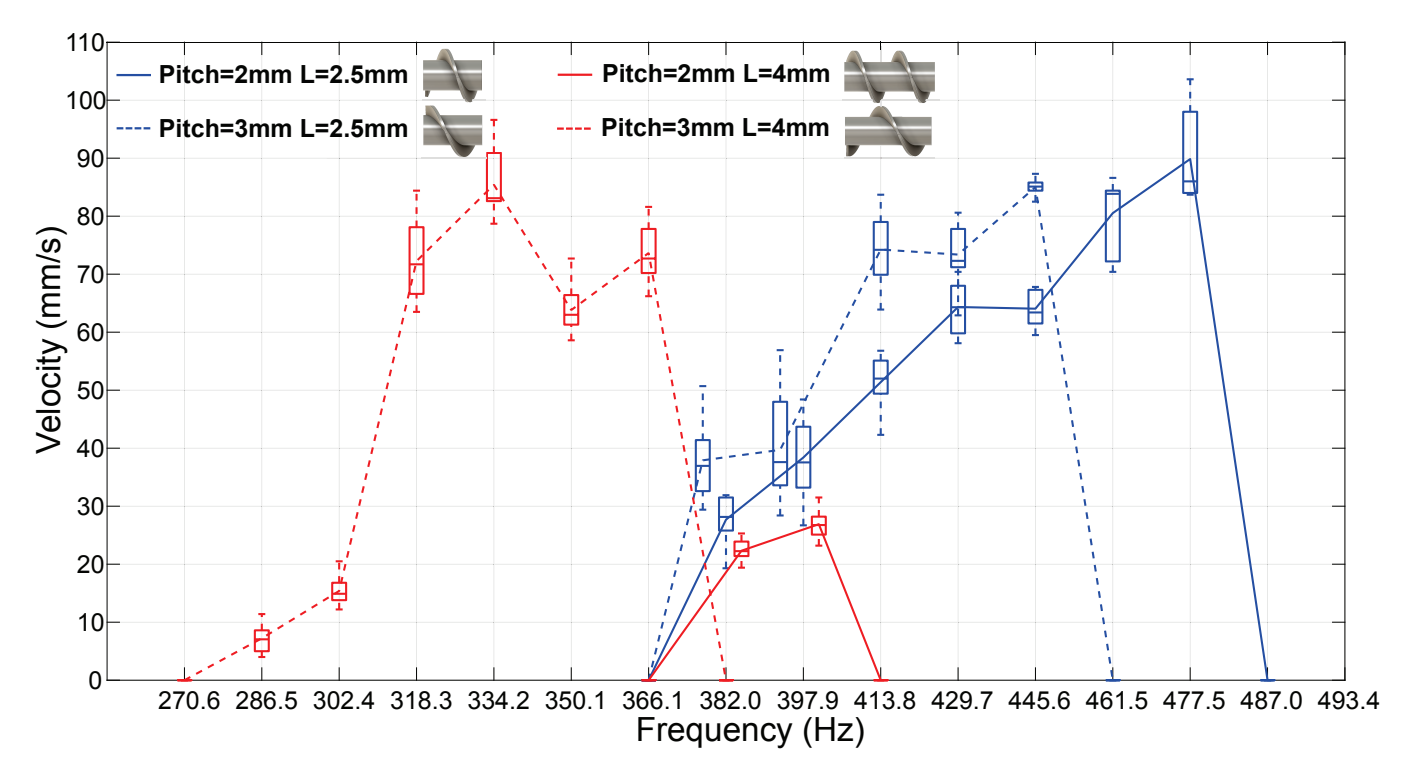


Fig. 4. Plot of the maximum linear velocity as a function of magnetic field rotational frequency for four swimmer geometries. Each box whisker icon represents 10 trials.

The trajectory following is accurate on the portion that goes up though the tube. The swimmer is able to go through the tube without touching the walls. On this part, the swimmer needs to compensate for its weight. The swimmer's velocity is dominated by the thrust vector which maximizes the control authority.

VI. EXPERIMENTAL OPTIMIZATION OF THE SWIMMER

Different swimmer designs were tested experimentally. Two different lengths (2.5 mm and 4 mm) as well as two different pitches (2 and 3 mm) were tested and compared. The velocity of each swimmer was obtained by measuring the time it takes the swimmer to go through the last 20 mm of the tube. Results of the velocity measurements are presented in fig. 4. Ten measurements were made for each rotational speed

The fastest swimmer has a pitch of 2 mm and a length of 2.5 mm. It is shown in fig. 3 (a). This swimmer climbed at an average speed of 90 mm/s with a maximum recorded velocity of 103.6 mm/s. The variation in velocity is explained by the fact that the controller must compensate perturbations to keep the swimmer on the centerline by slightly changing the orientation of the swimmer. The perturbations are not exactly the same for each loop achieved.

The maximum torque that the manipulator can apply was the same for each test. The applied torque is calculated using eq. 13. The angle between the applied magnetic field $\bf B$ and the magnetization $\bf m$ of the swimmer will be called internal angle (α_i) in this paper, similar to the terminology used for synchronous electric motors. The maximum torque is

reached when α_i reaches $\pi/2$ rad. If this angle is exceeded, the torque applied decreases. The angular velocity of the swimmer also decreases and is no longer equal to the rotational speed of the applied magnetic field. Under these conditions and in accordance with eq. 13, the average torque applied to the swimmer is equal to zero. The swimmer, therefore, stops rotating. The frequency that produces an internal angle equal to $\pi/2$ is called the *step-out frequency*.

$$\Gamma = \mathbf{m} \cdot \mathbf{B} \tag{13}$$

It is observed from the experimental curves that the stepout frequency is reduced when the swimmer length increases and when the pitch is increased. This is explained by the fact that, for a given rotational speed, the friction torque increases with the length of the swimmer. More surface area is in contact with the liquid. The torque also increases if the pitch is increased as the attack angle of the screw thread increases.

Since all swimmers have a diameter of 2.5 mm, their cross-section is, therefore, the same. For a given rotational speed, there is a maximum amount of liquid that can go through this surface area. It is equal to $S \cdot P \cdot \omega/(2\pi)$ where S is the cross-section area, P is the pitch and ω is the rotational speed. It can be seen on fig. 4 that the swimmer with a pitch of 2 mm and a length of 4 mm performs poorly. This can be explained by the fact that the increased length only moves slightly more liquid. However, this small increase does not compensate for the added weight. In addition, the friction torque produced for a given rotational speed is increased which in turn decreases the step-out frequency.

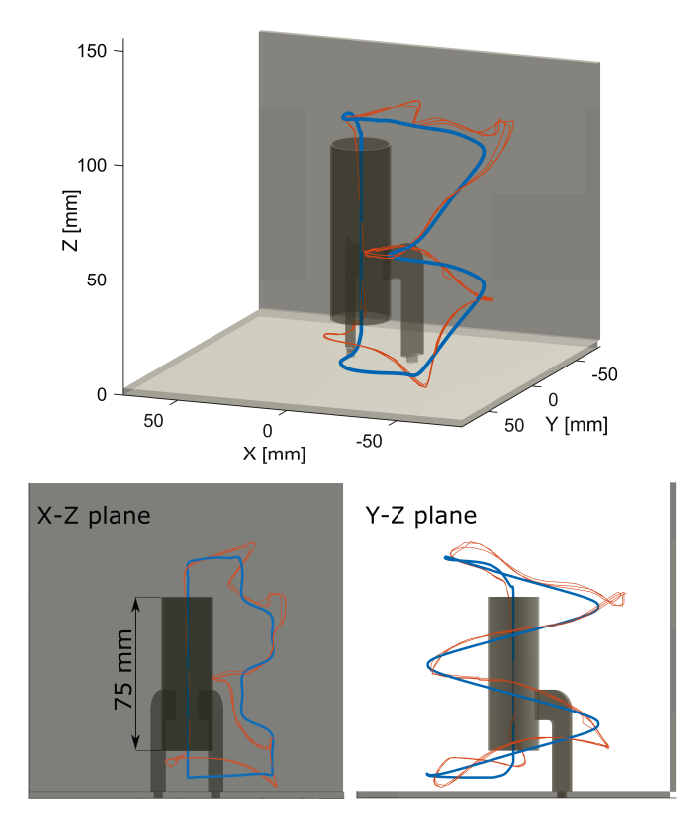


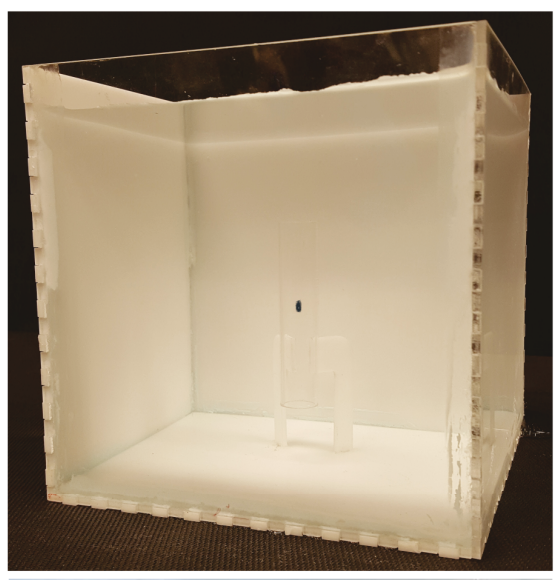
Fig. 5. Schematic representation of the trajectory following experiment. A transparent tube is used to simulate the aorta. The blue curve corresponds to the trajectory to follow. The orange curve shows the path executed experimentally by the swimmer while completing the trajectory three times.

VII. CONCLUSION AND FUTURE WORK

Millimeter-scale rotating magnetic swimmers have the potential to be used to remove occlusions inside arteries. 3D control of several magnetic swimmers was studied and experimentally tested. The swimmers are able to travel through a tube with a diameter of 15 mm. The tube simulates the aorta at its smallest diameter. The swimmers did not touch the walls of the tube during the navigation indicating that it may be possible to avoid accidentally detaching a plaque inside a real aorta.

Several designs were tested and compared. The best swimmer moves at an average vertical velocity of 90 mm/s with a maximum recorded speed of 103.6 mm/s.

These swimmers were tested inside water which has a viscosity of 0.89 mPa/s. However, human blood viscosity ranges from 2 to 3 mPa/s. Increased viscosity increases drag, so which will decrease the swimmer's speed. Future work will investigate the effect of increased viscosity on the performance of the swimmer. New swimmers will be optimized by computing the fluid dynamics using a 3D finite elements software. Navigation in a realistic pulsating blood flow should also be investigated. Techniques using a non optical tracking method are required. Design of appropriate end-effector tooling is also left for future work.



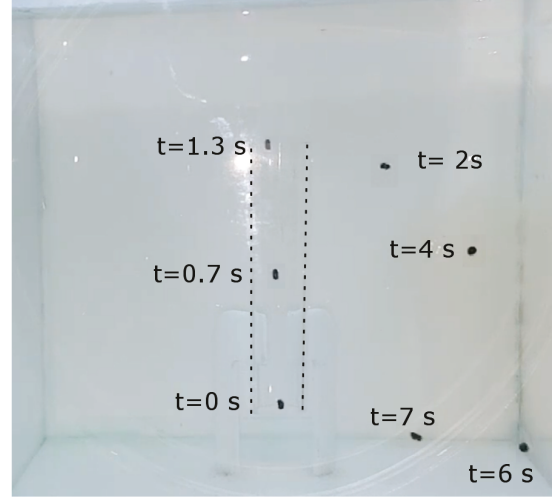


Fig. 6. Picture presenting the workspace with a tube simulating an aorta (top) and picture of the swimmer during the navigation (bottom). The workspace is a cube having a side length of 150 mm. The swimmer navigating has a length of 2.5 mm, a diameter of 2.5 mm and a pitch of 2 mm.

REFERENCES

- E. Zeitler, W. Schoop, and W. Zahnow, "The treatment of occlusive arterial disease by transluminal catheter angioplasty," *Radiology*, vol. 99, no. 1, pp. 19–26, 1971.
- [2] I. S. Khalil, A. F. Tabak, K. Sadek, D. Mahdy, N. Hamdi, and M. Sitti, "Rubbing against blood clots using helical robots: modeling and in vitro experimental validation," *IEEE Robotics and Automation Letters*, vol. 2, no. 2, pp. 927–934, 2017.
- [3] I. S. M. Khalil, D. Mahdy, A. E. Sharkawy, R. R. Moustafa, A. F. Tabak, M. E. Mitwally, S. Hesham, N. Hamdi, A. Klingner, A. Mohamed, and M. Sitti, "Mechanical rubbing of blood clots using helical robots under ultrasound guidance," *IEEE Robotics and Automation Letters*, vol. 3, no. 2, pp. 1112–1119, April 2018.
- [4] W. Lee, S. Jeon, J. Nam, and G. Jang, "Dual-body magnetic helical robot for drilling and cargo delivery in human blood vessels," *Journal* of Applied Physics, vol. 117, no. 17, p. 17B314, 2015.
- [5] F. Z. Temel and S. Yesilyurt, "Magnetically actuated micro swimming

- of bio-inspired robots in mini channels," in *Mechatronics (ICM)*, 2011 IEEE International Conference on. IEEE, 2011, pp. 342–347.
- [6] E. Diller, Z. Ye, and M. Sitti, "Rotating magnetic micro-robots for versatile non-contact fluidic manipulation of micro-objects," in 2011 IEEE/RSJ International Conference on Intelligent Robots and Systems, Sep. 2011, pp. 1291–1296.
- [7] F. Qiu, S. Fujita, R. Mhanna, L. Zhang, B. R. Simona, and B. J. Nelson, "Magnetic helical microswimmers functionalized with lipoplexes for targeted gene delivery," *Advanced Functional Materials*, vol. 25, no. 11, pp. 1666–1671, 2015.
- [8] H. Li, J. Tan, and M. Zhang, "Dynamics modeling and analysis of a swimming microrobot for controlled drug delivery," in *Robotics and Automation*, 2006. ICRA 2006. Proceedings 2006 IEEE International Conference on. IEEE, 2006, pp. 1768–1773.
- [9] W. Gao, X. Feng, A. Pei, C. R. Kane, R. Tam, C. Hennessy, and J. Wang, "Bioinspired helical microswimmers based on vascular plants," *Nano letters*, vol. 14, no. 1, pp. 305–310, 2013.
- [10] X. Yan, Q. Zhou, J. Yu, T. Xu, Y. Deng, T. Tang, Q. Feng, L. Bian, Y. Zhang, A. Ferreira, and L. Zhang, "Magnetite nanostructured porous hollow helical microswimmers for targeted delivery," *Advanced Functional Materials*, vol. 25, no. 33, pp. 5333–5342, 2015. [Online]. Available: https://onlinelibrary.wiley.com/ doi/abs/10.1002/adfm.201502248
- [11] S. Tottori, L. Zhang, F. Qiu, K. K. Krawczyk, A. Franco-Obregón, and B. J. Nelson, "Magnetic helical micromachines: fabrication, controlled swimming, and cargo transport," *Advanced materials*, vol. 24, no. 6, pp. 811–816, 2012.
- [12] A. Ghosh and P. Fischer, "Controlled propulsion of artificial magnetic nanostructured propellers," *Nano letters*, vol. 9, no. 6, pp. 2243–2245, 2009.
- [13] F. Ullrich, F. Qiu, J. Pokki, T. Huang, S. Pan, and B. J. Nelson, "Swimming characteristics of helical microrobots in fibrous environments," in 2016 6th IEEE International Conference on Biomedical Robotics and Biomechatronics (BioRob), June 2016, pp. 470–475.
- [14] S. Kim, K. Shin, S. Hashi, and K. Ishiyama, "A pushing force mechanism of magnetic spiral-type machine for wireless medicalrobots in therapy and diagnosis," *IEEE Transactions on Magnetics*, vol. 49, no. 7, pp. 3488–3491, 2013.
- [15] K. Ishiyama, K. Arai, M. Sendoh, and A. Yamazaki, "Spiral-type micro-machine for medical applications," in *Micromechatronics and Human Science*, 2000. MHS 2000. Proceedings of 2000 International Symposium on. IEEE, 2000, pp. 65–69.
- [16] H. Zhou, G. Alici, T. D. Than, and W. Li, "Modeling and experimental investigation of rotational resistance of a spiral-type robotic capsule inside a real intestine," *IEEE/ASME Transactions On Mechatronics*, vol. 18, no. 5, pp. 1555–1562, 2013.
- [17] M. Sendoh, K. Ishiyama, and K.-I. Arai, "Fabrication of magnetic actuator for use in a capsule endoscope," *IEEE Transactions on Magnetics*, vol. 39, no. 5, pp. 3232–3234, 2003.
- [18] A. W. Mahoney and J. J. Abbott, "Five-degree-of-freedom manipulation of an untethered magnetic device in fluid using a single permanent magnet with application in stomach capsule endoscopy," *The International Journal of Robotics Research*, vol. 35, no. 1-3, pp. 129–147, 2016.
- [19] G. Go, H. Choi, S. Jeong, C. Lee, S. Y. Ko, J. Park, and S. Park, "Electromagnetic navigation system using simple coil structure (4 coils) for 3-d locomotive microrobot," *IEEE Transactions on Magnetics*, vol. 51, no. 4, pp. 1–7, April 2015.
- [20] A. W. Mahoney, J. C. Sarrazin, E. Bamberg, and J. J. Abbott, "Velocity control with gravity compensation for magnetic helical microswimmers," *Advanced Robotics*, vol. 25, no. 8, pp. 1007–1028, 2011.
- [21] M. P. Kummer, J. J. Abbott, B. E. Kratochvil, R. Borer, A. Sengul, and B. J. Nelson, "Octomag: An electromagnetic system for 5-dof wireless micromanipulation," *IEEE Transactions on Robotics*, vol. 26, no. 6, pp. 1006–1017, 2010.
- [22] T. Xu, G. Hwang, N. Andreff, and S. Rgnier, "Characterization of three-dimensional steering for helical swimmers," in 2014 IEEE International Conference on Robotics and Automation (ICRA), May 2014, pp. 4686–4691.
- [23] T. Xu, G. Hwang, N. Andreff, and S. Rgnier, "Planar path following of 3-d steering scaled-up helical microswimmers," *IEEE Transactions* on *Robotics*, vol. 31, no. 1, pp. 117–127, Feb 2015.
- [24] https://youtu.be/qMR0tZabKk8.

- [25] "Boston scientific," https://www.bostonscientific.com/, accessed: 2018-09-15.
- [26] J. Leclerc, B. Isichei, and A. T. Becker, "A magnetic manipulator cooled with liquid nitrogen," *IEEE Robotics and Automation Letters*, vol. 3, no. 4, pp. 4367–4374, Oct 2018.
- [27] "National instruments," http://www.ni.com, accessed: 2018-09-15.
- [28] "Basler," https://www.baslerweb.com/, accessed: 2018-09-15.
- [29] Q. Pan, S. Guo, and T. Okada, "Mechanism and control of a spiral type microrobot," in *The 2010 IEEE International Conference on Information and Automation*, June 2010, pp. 735–740.
- [30] K. Ishiyama, K. I. Arai, M. Sendoh, and A. Yamazaki, "Spiral-type micro-machine for medical applications," in MHS2000. Proceedings of 2000 International Symposium on Micromechatronics and Human Science (Cat. No.00TH8530), Oct 2000, pp. 65–69.
- [31] "3d systems," https://www.3dsystems.com, accessed: 2018-09-14.